Reviewed Preprint
v1 • August 21, 2026
Not revised

For correspondence:
lidan@zjut.edu.cn

* These authors contributed equally.

Competing interests: No competing interests declared

Funding: See page 14

Reviewing editor: Arya Mani, Yale University School of Medicine, United States

Targeting Lysosomal MCOLN1/TRPML1 Ion Channels to Finely Alleviate Diabetes Mellitus via a Ca^{2+}- CaMKKβ-AMPK pathway

Jiaxuan Zhu[1,*], Zhaonan Pan[1,*], Shijia Wang[1,*], Yuyuan Wang[1], Zongxian Ding[1], Qianhui Wang[1], Dan Li[1,2]

[1]Collaborative Innovation Center of Yangtze River Delta Region Green Pharmaceuticals, College of Pharmaceutical Sciences, Zhejiang University of Technology, Hangzhou, China • [2]Department of Molecular, Cellular, and Developmental Biology, University of Michigan, Ann Arbor, United States

eLife Assessment

This study presents **valuable** evidence that activating a lysosomal signaling pathway lowers blood glucose in diabetic mice, pointing to a potential new strategy for treating metabolic disease. However, the evidence for the proposed mechanism is **inadequate**: the glucose transporter's movement and glucose uptake were not measured in the physiologically relevant tissue, and the measurement that was performed used an unconventional technique. As a result, whether this transporter-dependent pathway explains the glucose-lowering effect has not yet been established.

https://doi.org/10.7554/eLife.112056.1.sa3

Abstract

Type 2 Diabetes mellitus (T2DM) is a metabolic syndrome characterized by hyperglycemia and various complications. Current drugs are limited by side effects and resistance, necessitating novel targets and therapies. Previous studies have shown that MK-83, a synthetic agonist of transient receptor potential mucolipin 1 (TRPML1/ MCOLN1), a lysosomal Ca^{2+} channel, activates adenosine 5'-monophosphate-activated protein kinase (AMPK), a key therapeutic target in diabetes. However, whether targeting TRPML1 can treat T2DM remains unclear. In this study, we found that transgenic overexpression or pharmacological activation of TRPML1 finely controls AMPK phosphorylation via a Ca^{2+}-CaMKKβ-dependent mechanism. This activation promotes glucose transporter 4 (GLUT4) translocation and dramatically increases intracellular glucose uptake. Conversely, genetic inactivation or pharmacologically inhibition of TRPML1 blocks both AMPK activation and glucose uptake. More importantly, pharmacological activation of TRPML1 *in vivo* dramatically alleviates hyperglycemia in db/db mice (a T2DM model), as evidenced by random blood glucose levels, fasting blood glucose levels and HbA1c levels. Furthermore, other hallmark features of db/db mice-including impaired oral glucose tolerance, reduced insulin tolerance, and elevated ALT and AST levels- were all ameliorated upon TRPML1 activation. Hence, targeting lysosomal TRPML1 channel represents a promising therapeutic strategy for T2DM, with highly specific TRPML1 agonists as potential anti-diabetic agents.

Introduction

Type 2 diabetes mellitus (T2DM) is a chronic disease, characterized by hyperglycemia and relative insulin deficiency that affects more than 400 million people worldwide [1]. Despite the wide range of available antidiabetic drugs, side effects, drug resistance, and patient heterogeneity highlight the urgent need for new therapeutics with novel mechanisms to address clinical needs [2]. Eukaryotes possess a conserved signaling pathway that responds to low cellular ATP (due to

reduced oxygen or glucose) by activating adenosine monophosphate-activated protein kinase (AMPK) [3], which then phosphorylates key targets to regulate lipid and glucose metabolism [4]. Given that AMPK is essential for glucose homeostasis [3], it represents a key therapeutic target for diabetes and related metabolic diseases. Mechanistically, AMPK is activated when its α-subunit is phosphorylated at Thr172 by upstream kinases via energy- or Ca^{2+}-dependent pathways [3, 5]. Once activated, AMPK suppresses anabolic (energy-consuming) processes and promotes catabolic (energy-producing) ones [6]. In nutrient-rich conditions, ATP binds to the γ subunit of AMPK and keeps it inactive. Under energetic stress, AMP replaces ATP, triggering liver kinase B1 (LKB1) to phosphorylate the α subunit of AMPK.

Notably, cytoplasmic Ca^{2+} can activate AMPK independently of cellular energy status [5, 7]. Lysosomes, mitochondria and endoplasmic reticulum (ER) are the main intracellular Ca^{2+} stores [8] and some connections between distinct cytosolic Ca^{2+} sources and AMPK activation have been investigated [9]. Nevertheless, the involvement of lysosomes in AMPK activation and its implications for treating diabetes and metabolic diseases have yet to be elucidated. Transient Receptor Potential Mucolipin 1 (MCOLN1/TRPML1) is the best characterized lysosomal Ca^{2+} channel, mediating Ca^{2+} release from the lumen to the cytosol. TRPML1 dysfunction underlies various metabolic diseases, lysosomal storage diseases and neurodegenerative disorders [10–12]. For example, mutations in the gene encoding TRPML1 cause mucolipidosis type IV (MLIV), a lysosomal storage disease characterized by early-onset progressive neurodegeneration [13]. Lysosomal dysfunction is closely associated with multiple metabolic diseases, including obesity, T2DM, non-alcoholic fatty liver disease, and atherosclerosis [14, 15]. Impaired lysosomal function disrupts lipid metabolism, autophagy, and inflammation, leading to insulin resistance and β-cell failure [16].

Previous studies have shown that the synthetic TRPML1 agonist MK6-83 activates AMPK in human fibroblasts [9]. However, whether the TRPML1–AMPK axis regulates glucose metabolism, particularly in the context of T2DM, remains unclear. To address this, the current study investigates how TRPML1 activation regulates glucose metabolism, and ML-SA8, a TRPML1 agonist with higher *in vitro* potency (ML-SA8>ML-SA5 > MK6-83) [17–19], was applied to elucidate the therapeutic effects and molecular mechanisms of TRPML1 activation in T2DM models.

In the current proof-of-concept study, we found that both genetic and pharmacological activation of the lysosomal TRPML1 channel are sufficient to activate AMPK and alleviate diabetic phenotypes *in vitro* and *in vivo*. Therefore, we propose that pharmacological activation of TRPML1 may serve as a potential therapeutic strategy for T2DM.

Results

Pharmacological activation of lysosomal TRPML1 induces AMPK activation

Cytosolic Ca^{2+} reportedly activates AMPK [20, 21]. Lysosome, mitochondria and ER are the major compartmentalized Ca^{2+} stores in cells [8]; the mechanistic links between cytosolic Ca^{2+} and AMPK activation lead us to consider the discrete Ca^{2+} sources as a potential specificity determinant of AMPK activation [22, 23]. In this study, we investigated whether lysosome-released ions can activate AMPK, whose activation was measured by the phosphorylation status of threonine 172 (referred as Thr172) [24].

TRPML1 is the principal Ca^{2+}-permeable channel that releases Ca^{2+} from the lumen into the cytosol upon cellular stimulation [25, 26].Thus we then investigated whether TRPML1 contributes to AMPK activation. Although the synthetic TRPML1 agonist MK6-83 was previously shown to activates AMPK in human fibroblasts [9], here we used a much more potent TRPML1 agonist, ML-SA8 [27] (EC_{50}=0.086 ± 0.013 μM for endogenous TRPML1; Suppl. Fig. 1a, b). As shown in Fig. 1a, b, ML-SA8 (0.3-3 μM, 2 h) induces robust AMPK phosphorylation in a dose-dependent manner in HepG2 cells as well as several other cell lines including HeLa (Suppl. Fig. 1c, d) and HAP1 (Suppl. Fig. 1e, f). And this activation by ML-SA8 was completely blocked by dorsomorphin/compound C

(CC, 10 μM, an AMPK inhibitor [28]) (Fig. 1c, d). Similarly, AMPK can be activated by another less potent TRPML1 agonist ML-SA5 (potency SA8> SA5>MK6-83 [18, 27, 29]) in HepG2, HeLa and HAP1 cells (Suppl. Fig. 2a-c). Note that the specificities of ML-SAs have been previously validated using TRPML1 knockout (KO) cells [18, 29] and confirmed in the atomic-resolution co-structures [30, 31]. In addition, we investigated the role of another lysosomal Ca^{2+} channel, TPC2, using its specific agonist riluzole [25]. As shown in Suppl. Fig. 3a, b; AMPK activation required 800 μM of riluzole, a concentration exceeding its physiological range [32–35]. Therefore, we focused our research on ML-SA8-induced AMPK phosphorylation.

Glucose transporters (GLUTs) at the plasma membrane reportedly facilitate glucose uptake by an inward diffusion gradient for glucose [36]. In particular, GLUT4 is known to participate in AMPK-mediated glucose uptake by translocating from cytoplasm to plasma membrane [37]. Although GLUT4 is not the predominant GLUT isoform in the liver, it is nevertheless expressed in this organ [38–40]. Therefore, we next investigated whether ML-SA8 regulates the translocation of GLUT4. As shown in Fig. 1e, ML-SA8 (1 μM) induced a substantial increase in GLUT4 protein at the plasma membrane (PM) of HepG2 cells by immunofluorescence, indicating that ML-SA8 promotes GLUT4 translocation to the PM. Moreover, we isolated PM and post-PM fractions (supernatants devoid of PM) from HepG2 cells treated with ML-SA8 or vehicle control. Quantification of GLUT4 levels in the PM fraction confirmed that ML-SA8 stimulated GLUT4 translocation (Fig. 1f, g). Moreover, ML-ML-SA8 upregulated the expression level of GLUT4 in HepG2 cells (Suppl. Fig. 4). Collectively, these finding indicate that ML-SA8 promotes both PM translocation and the expression of GLUT4.

We then studied the effect of ML-SA8 on glucose levels by measuring both cellular glucose uptake and glucose consumption in the medium [41]. First, we constructed a palmitic acid (PA)-induced insulin resistance (IR) cell model [42, 43]. As shown in Suppl. Fig. 5a, b, insulin (100 nM, 0.5 h) induced glucose influx in HepG2 cells measured by 2-deoxy-2-[(7-nitro-2,1,3-benzoxadiazol-4-yl)amino]-d-glucose (2-NBDG), a fluorescent glucose analog, which is transported into cells and phosphorylated by hexokinase, trapping it intracellularly and allowing fluorescence-based quantification of glucose uptake [44]. In contrast, in PA (0.25 mM, 12 h)-treated HepG2 cells, insulin (100 nM, 0.5 h)-induced glucose influx was almost completely blocked, suggesting that PA-treated HepG2 cells are less sensitive to insulin (Thereafter IR-HepG2 represents PA-induced insulin resistant HepG2 cells). ML-SA8 (1 μM, 2 h)-induced AMPK phosphorylation was validated in IR-HepG2 cells by western blot analysis (Suppl. Fig. 5c). In IR-HepG2 cells, we observed that upon ML-SA8 (0.1-3 μM, 2-6 h) treatment, the intensities of 2-NBDG were dramatically increased compared to control in a dose- (Fig. 1h, i) and time-dependent (Suppl. Fig. 5d, e) manner. Correspondingly, glucose consumption in the culture medium was dramatically decreased with ML-SA8 (1 μM, 4 h) treatment in IR-HepG2 cells (Fig. 1j). Likewise, ML-SA8 (1 μM) was sufficient to induce cellular glucose uptake in various cells such as human hepatocellular carcinoma cells (Huh7) and mice myoblast cells (C2C12) following IR (PA-treated) induction (Suppl. Fig. 5f, g). Taken together, these data demonstrated that stimulation of TRPML1 activates AMPK signaling cascades, which facilitates GLUT4 PM translocation, leading to the increases of cellular glucose uptake.

TRPML1 is essential in ML-SA-induced AMPK activation

We then investigated whether increasing the expression of TRPML1 in HepG2 cells is sufficient to increase the cells' sensitivity to ML-SA8 treatment. Remarkably, a low dose of ML-SA8 (0.03 μM) can activate AMPK in HepG2 cells overexpressing GFP-TRPML1, but not in wild type (WT) cells (Fig. 2a). Consistently, ML-SA8 (0.03 μM) can also promote cellular glucose uptake in TRPML1-overexpressing IR-HepG2 cells (Fig. 2b, c), while no such effects were observed in IR-HepG2 cells. Collectively, these data demonstrate that the TRPML1 overexpression can promote AMPK activation.

Next, we investigated whether TRPML1 is required for ML-SA-induced AMPK activation using the TRPML1 specific synthetic inhibitor-ML-SI5, whose specificities have been previously validated [17, 27]. Pretreatment with ML-SI5 (3 μM) completely abolished ML-SA8-triggered (1 μM, 2 h)

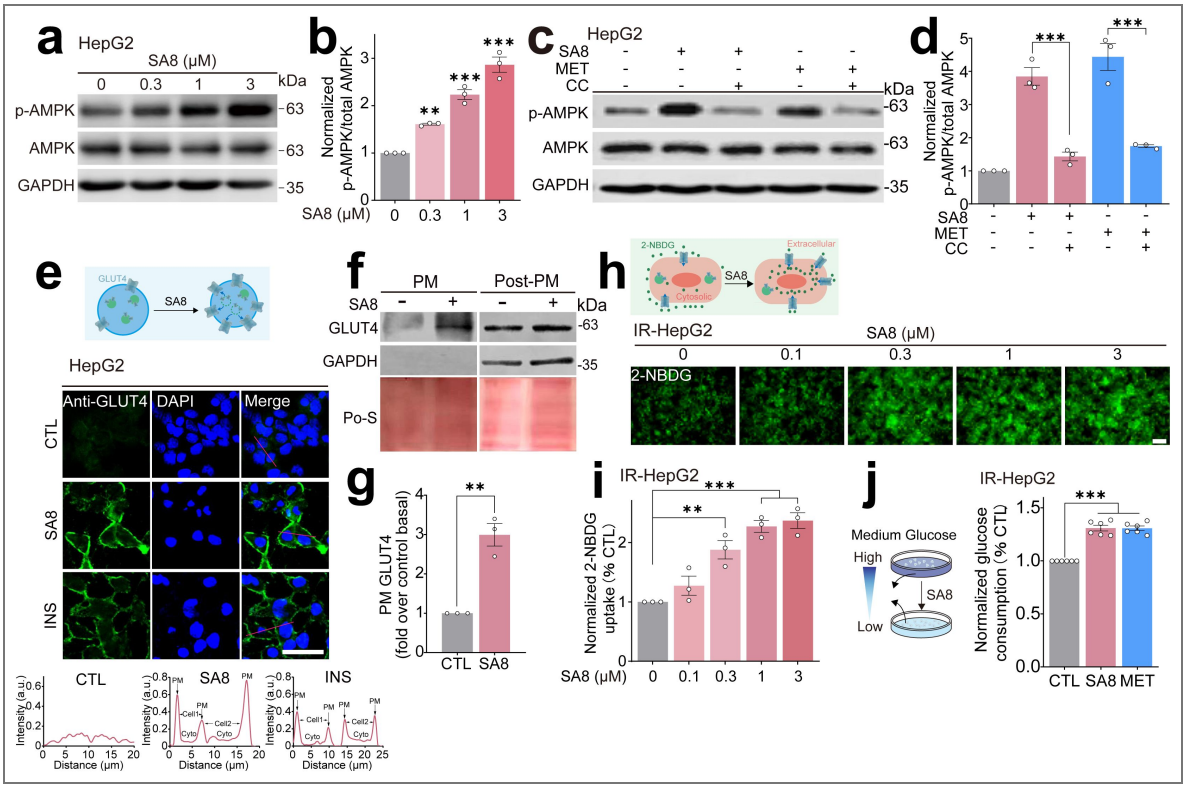

Figure 1. Stimulation of the lysosomal TRPML1 channel induces AMPK activation.

(**a**) ML-SA8 (a TRPML1 specific synthetic agonist) activated AMPK in a dose-dependent manner. HepG2 cells were treated with ML-SA8 (0.3-3 μM) for 2 h. (**b**) Quantification of results shown in **c.** from n= 3 independent experiments. **(c)** AMPK inhibitor blocked ML-SA8-induced AMPK phosphorylation. HepG2 cells were pretreated with CC (10 μM, 1h), followed by cotreatment with ML-SA8 (1 μM, 2 h) and AMPK phosphorylation was measured by Western blotting. **(d)** Ratio of p-AMPK/total AMPK shown in **e.** (n= 3). (**e**) ML-SA8 induced GLUT4 PM translocation. HepG2 cells were treated with ML-SA8 (1 μM, 4 h) and GLUT4 immunoreactivity was measured. Nuclei were counterstained with DAPI (blue). Scale bar, 20 μm. The graph at the *Righter* panel shows the fluorescence intensity of GLUT4 with a red line scan across a cell (red line shown in the *Lefter* images). (**f**) Western blot analysis of PM GLUT4 expression induced by ML-SA8. Membrane and cytoplasm protein fractions were isolated from cells treated with ML-SA8 (1 μM) or DMSO for 4 h and subjected to western blot analysis. (**g**) Quantification of PM GLUT4 expression as shown in **f**. (n= 3 independent experiments). (**h**) ML-SA8 promoted glucose influx. IR-HepG2 cells were treated with ML-SA8 (0.1-3 μM) for 4 h, followed by 2-NBDG (50 μM, 0.5 h) treatment. Scale bar, 40 μm. (**i**) Quantification of the relative fluorescent intensity of 2-NBDG in **h.** from n= 3 independent experiments. (**j**) The effect of ML-SA8 on glucose consumption in medium. IR-HepG2 cells were treated with or without ML-SA8 (1 μM) for 4 h in DMEM containing 10 mM glucose, no FBS, no phenol red, and glucose consumption in the medium was measured. Metformin (MET, 2 mM) served as a positive control. For all panels, data are presented as mean ± s.e.m.; *$p < 0.05$, **$p < 0.01$, ***$p < 0.001$, ANOVA.

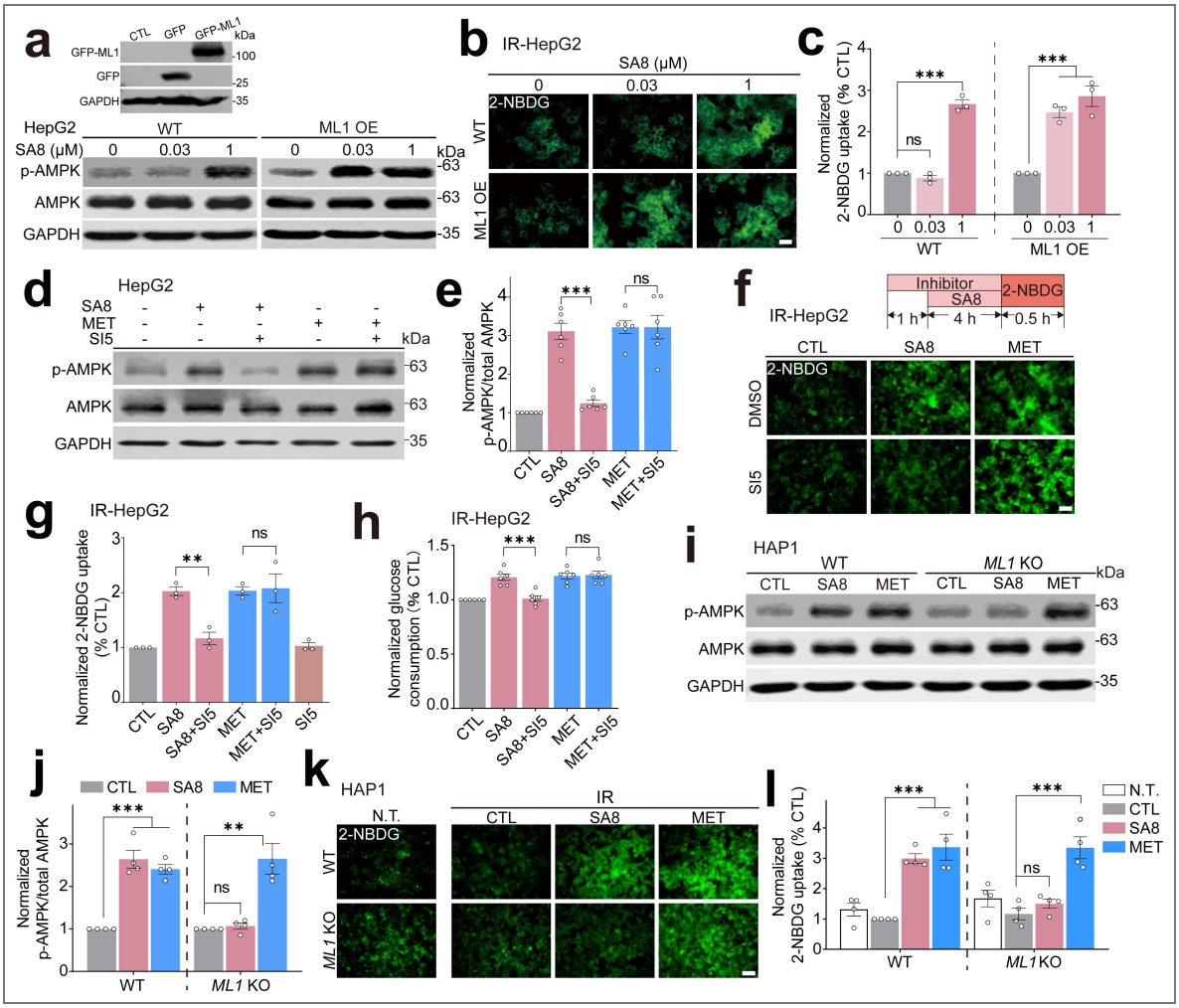

Figure 2. TRPML1 is required for ML-SA8-induced AMPK activation.

(a) Overexpressing *TRPML1* further promoted low-dose of ML-SA8- activating AMPK. In the top panel, western blot validation of the GFP-TRPML1 overexpression in HepG2. In the bottom panel, HepG2 cells with or without GFP-TRPML1 overexpression were treated with ML-SA8 (0.03-1 μM) for 2 h and western blotting analysis of p-AMPK/total AMPK protein levels. **(b)** TRPML1 overexpression promoted cellular glucose uptake (2-NBDG) by low-dose of SA8 (0.03-1 μM, 4 h) in IR-HepG2 cells. Scale bar, 40 μm. **(c)** Quantification of the relative fluorescent intensity of 2-NBDG shown in **b.** (n= 3 independent experiments). (**d**) ML-SI5 (a TRPML1 synthetic inhibitor) blocked ML-SA8-induced AMPK activation. Western blot analysis of AMPK phosphorylation in HepG2 cells pretreated with ML-SI5 (3 μM) for 1 h, followed by cotreated with ML-SA8 (1 μM) or MET (2 mM) for 2 h. (**e**) Quantification of the results shown in **d.** from n= 6 independent experiments. (**f**) The effect of ML-SI5 on ML-SA8-induced cellular glucose uptake. IR-HepG2 were pretreated with ML-SI5 (3 μM) for 1 h, then cotreated with ML-SA8 (1 μM, 4 h), followed by 2-NBDG (50 μM, 0.5 h). Scale bar, 40 μm. (**g**) Quantification of the intensity of 2-NBDG in **f.** (n= 3). (**h**) ML-SI5 blocked ML-SA8-induced glucose consumption. IR-HepG2 cells were pretreated with ML-SI5 (3 μM) for 1 h, then cotreated with ML-SA8 (1 μM) or MET (2 mM) for 4 h, finally glucose levels in the supernatant medium were measured. (**i**) Western blotting analysis of p-AMPK levels in WT and *TRPML1* KO HAP1 cells treated with ML-SA8 (1 μM) or MET (2 mM) for 2 h. (**j**) Quantitative analysis of p-AMPK/total AMPK levels as shown in **i.** from n= 4 independent experiments. (**k**) *TRPML1* KO abrogated ML-SA8- but not MET-induced cellular glucose uptake. WT and *TRPML1* KO HAP1 cells were treated with PA (0.25 mM, 12 h), followed by ML-SA8 (1 μM) or MET (2 mM) for 4 h. 2-NBDG (50 μM, 0.5 h) was then applied and measured. Scale bar, 40 μm. (**l**) Quantification of the relative fluorescent intensity of 2-NBDG in **k.** from n= 4 independent experiments. In all panels, data are presented as mean ± s.e.m.; $^{**}p < 0.01$, $^{***}p < 0.001$.

AMPK phosphorylation, while no effect on metformin (MET)-induced AMPK activation (Fig. 2d, e). Moreover, in IR-HepG2 model, ML-SI5 substantially inhibited ML-SA8-, but not MET-induced cellular glucose uptake and extracellular glucose consumption (Fig. 2f-h). To further validate the TRPML1-dependent mechanism, we utilized a *TRPML1* knockout (KO) HAP1 cell line constructed by CRISPR-Cas9 as previously described [45]. In *TRPML1* KO HAP1 cells, ML-SA8 (1 μM, 2 h)-induced AMPK phosphorylation and cellular glucose uptake were almost completely abolished compared to wild-type (WT) HAP1 cells (Fig. 2i-l). Collectively, these data demonstrate that TRPML1 is both sufficient and necessary for ML-SA-induced AMPK activation in IR model cells.

Ca^{2+} -CaMKKβ -dependence of ML-SA-induced AMPK activation

Lysosomal TRPML1 is a non-selective cation channel that is permeable to Ca^{2+}, as well as heavy metal ions such as Fe^{2+} and Zn^{2+} [46]. Given the well-established role of Ca^{2+} in AMPK activation [47], we first examined whether Ca^{2+} is required for ML-SA's AMPK activation upon TRPML1 stimulation. BAPTA-AM (20 μM), a membrane-permeable Ca^{2+} chelator (fast-acting) [48] readily blocked ML-SA8-evoked AMPK activation (Fig. 3a, b) and cellular glucose uptake (Fig. 3c, d). In contrast, EGTA-AM, another Ca^{2+} chelator (slow-acting), failed to block ML-SA8's effects (Fig. 3a-d). The inhibitory effects of BAPTA-AM (20 μM) and EGTA-AM (20 μM) on cytosolic Ca^{2+} was confirmed in HEK293 cells overexpressing GCaMP7-TRPML1 (Suppl. Fig. 6a). Considering that BAPTA has much faster Ca^{2+} association and dissociation kinetics than EGTA [49], this disparate Ca^{2+}-dependent mechanism suggests that ML-SA8-regulated AMPK cascades through a fast and local Ca^{2+} signal from lysosomes. Next, we examined whether Fe^{2+} and Zn^{2+} involve in ML-SA-triggered AMPK cascades. TPEN (10 μM), a high-affinity Zn^{2+} chelator [50], and deferoxamine (DFO) (10 μM), a Fe^{2+} chelator [51], both failed to block ML-SA8-induced AMPK activation and cellular glucose uptake (Suppl. Fig. 6b-e). Together, these data suggest that TRPML1 activation regulates AMPK-GLUT4-glucose pathway via a fast Ca^{2+} release from lysosomes.

We next investigated how ML-SA8 induces AMPK phosphorylation. A key mechanism of AMPK activation involves phosphorylation of its subunit at Thr172 site by upstream kinases, including CaMKKβ (calcium/calmodulin-dependent protein kinase kinase β which responds to elevated cytosolic Ca^{2+} [52, 53] and LKB1 [7]. Considering our finding that TRPML1-dependent Ca^{2+} release is essential for AMPK activation (Fig. 3a-d), we hypothesize that CaMKKβ serves as the critical upstream kinase bridging lysosomal Ca^{2+} signaling and ML-SA8-stimulated AMPK activation. Notably, STO609 (a CaMKKβ inhibitor, 10 μM) [54] significantly suppressed ML-SA8-induced AMPK phosphorylation in HepG2 cells (Fig. 3e, f). Furthermore, the effects of ML-SA8 on cellular glucose uptake (2-NBDG) were completely blocked by STO609 or CC (Fig. 3g, h). To further validate these findings, a genetic knockdown approach was employed. Consistent with the pharmacological inhibition, CaMKKβ knockdown markedly attenuated ML-SA8-induced AMPK phosphorylation (Fig. 3i, j) and abolished the associated increases in glucose uptake and extracellular glucose consumption (Fig. 3k–m). Collectively, these findings establish CaMKKβ as an essential upstream mediator required for AMPK activation and the improved glucose metabolism following ML-SA8 treatment.

Overall, these *in vitro* experiments demonstrate that pharmacological activation of TRPML1 stimulates AMPK via a Ca^{2+}-CaMKKβ-dependent pathway, thereby promoting GLUT4 translocation to the PM. This process enhances intracellular glucose uptake and helps maintain glucose homeostasis in a hepatic IR model (Fig. 3n).

TFEB-independence of ML-SA-induced AMPK activation

TRPML1 activation is known to upregulate lysosomal biogenesis through TFEB activation [48, 55, 56]. While AMPK reportedly mediates phosphorylation of TFEB, and its transcriptional activity [57]. TFEB belongs to the microphthalmia (MiT/TFE) family, which also contains TFE3 and MITF, contributing to autophagic and lysosomal biogenesis [55, 58]. Hence, we examined whether TFEB/TFE3/MITF participates in TRPML1 stimulation-induced AMPK activation by using *TFEB/TFE3/MITF* triple KO (TKO) cells. The efficiency of *TFEB/TFE3/MITF* TKO was confirmed by Western blotting with anti-TFEB, TFE3 and MITF specific antibodies (Suppl. Fig. 6a). We found

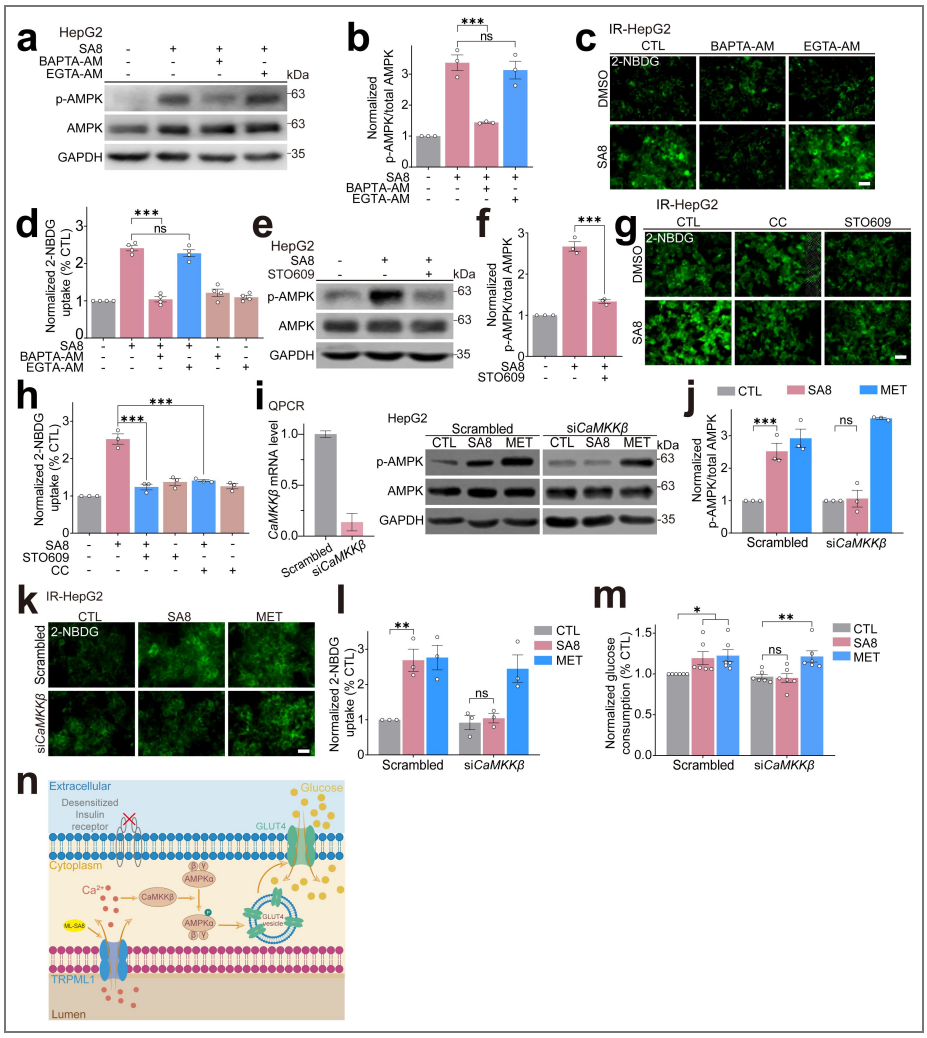

Figure 3. **Ca^{2+}- CaMKKβ dependence of ML-SA8 induced-AMPK activation.**

(a) BAPTA-AM inhibited ML-SA8-induced AMPK phosphorylation. HepG2 cells were pretreated with BAPTA-AM (fast Ca^{2+} chelator, 20 μM) or EGTA-AM (slow Ca^{2+} chelator, 20 μM) for 1 h, then cotreated with ML-SA8 (1 μM, 2 h), AMPK phosphorylation was then evaluated by Western blotting. **(b)** Quantification of results shown in **a.** from n= 3 experiments. **(c)** The effect of BAPTA-AM on ML-SA8-induced cellular glucose uptake. IR-HepG2 cells were treated with ML-SA8 (1 μM, 4 h) in the presence or absence of BAPTA-AM (20 μM) or EGTA-AM (20 μM), followed by analysis of cellular glucose levels with 2-NBDG. Scale bar, 40 μm. **(d)** Quantification of results shown in **c.** from (n= 4). **(e)** CaMKKβ inhibitor blocked ML-SA8-induced AMPK phosphorylation. HepG2 cells were pretreated with STO609 (10 μM, 1h) and cotreated with ML-SA8 (1 μM, 2 h), and AMPK phosphorylation was assayed by Western blotting. **(f)** Ratio of p-AMPK/total AMPK shown in **e.** (n= 3). **(g)** CC and STO609 abolished ML-SA8-induced cellular glucose uptake. IR-HepG2 cells were treated with ML-SA8 (1 μM) with or without CC (10 μM) or STO609 (10 μM) for 4 h and cellular glucose levels were measured by 2-NBDG. Scale bar, 40 μm. **(h)** Quantification of the intensity of 2-NBDG shown in **g.** (n= 3). **(i)** CaMKKβ KD abolished ML-SA8- induced AMPK activation. CaMKKβ KD efficiency was examined by QPCR (*Left panel*). HepG2 cells were transfected with CaMKKβ siRNA and then treated with ML-SA8 (1 μM) or MET (2 mM) for 2 h, then p-AMPK levels were measured by Western blot. **(j)** Quantitation of results shown in **i**. **(k)** CaMKKβ KD abrogated ML-SA8- induced cellular glucose uptake. IR-HepG2 cells were treated with ML-SA8 (1 μM) or MET (2 mM) for 4 h. 2-NBDG (50 μM, 0.5 h) was then applied and measured. Scale bar, 40 μm. **(l)** Quantification of results in **k**. (n= 3) **(m)** The effects of CaMKKβ KD on ML-SA8-induced glucose consumption. IR-HepG2 cells were treated with ML-SA8 (1 μM) or MET (2 mM) for 4 h, then glucose levels in the supernatant medium were measured (n=3). **(n)** A working model to illustrate that small-molecule TRPML1 agonist-ML-SA8 promotes cellular glucose uptake via TRPML1-Ca^{2+}-CaMKKβ-AMPK-GLUT4 pathway. ML-SA8 specifically activates TRPML1 channel, which releases Ca^{2+} into the cytoplasm. Elevated cytosolic Ca^{2+} then triggers CaMKKβ kinase activation, which phosphorylates AMPK to initiate its catalytic activity, followed by promoting GLUT4-containing vesicle translocation to the PM. Membrane-inserted GLUT4 facilitates extracellular glucose uptake into cells, ultimately restoring glycemic homeostasis. Arrows denote sequential signaling events, with color-coded molecular entities matching experimental annotations.

that in TKO cells, upon ML-SA8 (1 μM, 2 h) treatment, the increase of intensity of p-AMPK/total AMPK was not affected (Suppl. Fig. 7b, c), suggestive of TFEB/TFE3/MITF-independence of ML-SA8-triggered AMPK activation.

Next, we also assessed the role of AMPK in TRPML1 activation-mediated TFEB activity. Consistent with previous studies [18], ML-SA8 treatment (1 μM, 4 h) led to GFP-TFEB translocation from cytosol to nuclei in HeLa GFP-TFEB stable cells (Suppl. Fig. 7d, e), and this effect can be blocked by ML-SI5 treatment. However, CC or STO609 treatment failed to block ML-SA8-induced TFEB nuclear translocation (Suppl. Fig. 7d, e), suggesting that AMPK is dispensable for TRPML1 activation-induced subcellular TFEB translocation. Taken together, these results suggest that ML-SA8 -induced TFEB nuclear translocation is AMPK-independent.

Administration of ML-SA8 ameliorates diabetic phenotypes in db/db mice

Hepatic steatosis is strongly associated with T2DM and is considered as an exacerbating factor of hepatic insulin resistance. We next investigated whether the small-molecule TRPML1 agonist ML-SA8 could alleviate diabetic phenotypes in C57BLKS/J-Lepr KO (*db/db*) mice, a well-established diabetic mouse model [59]. To determine whether ML-SA8 targets/activates AMPK *in vivo*, 9-week-old *db/db* mice were intraperitoneally (i.p.) injected with ML-SA8 (4 mg/kg) or vehicle (5% DMSO, 90% PEG300, 5% ddH_2O). After 24 h, liver tissues were collected and pT172-AMPK/AMPK levels were measured by western blotting. As shown in Fig. 4a, b, ML-SA8 treatment significantly increased pT172-AMPK protein levels in liver tissues compared to vehicle, demonstrating that ML-SA8 activates AMPK in the liver of *db/db* mice.

We next evaluated the *in vivo* therapeutic efficacy of ML-SA8. 9-week- old *db/db* mice were randomly divided into three groups and treated daily for 6 weeks: 1) Vehicle group (DB+V): i.p. injection of vehicle (5% DMSO, 90% PEG300, 5 % ddH_2O); 2) ML-SA8 group (DB+SA8) : i.p. injection of ML-SA8 at 2, 4, 8 mg/kg. We further validated the targeting of AMPK in various tissues by 6-week treatment of ML-SA8. ML-SA8 induced AMPK phosphorylation levels in liver (Suppl. Fig.8a), as well as in adipose (Suppl. Fig.8b) and skeletal muscle tissues (Suppl. Fig.8c) in *db/db* mice. Moreover, GLUT4 protein expression significantly increased in liver of *db/db* mice treated with ML-SA8 by western blot (Fig. 4c, d) and immunofluorescence analysis (Suppl. Fig.8d). Furthermore, administration of SA8 (4 and 8 mg/kg) significantly reduced fasting blood glucose (FBG) levels (Fig. 4f), HbA1c levels (Fig. 4g) and random blood glucose (RBG) levels (Suppl. Fig.8e), oral glucose tolerance tests (OGTT) (Fig. 4h) and insulin tolerance test (ITT) (Fig. 4i). These data suggests that ML-SA8 reduced plasma glucose levels and increased the insulin sensitivity in *db/db* mice. Histological staining analysis showed that liver tissues in DB+V mice exhibited hepatic steatosis, lipid droplet accumulation, hepatocyte swelling and ballooning (Fig. 4j). In contrast, administration of SA8 (4 mg/kg) in DB mice was sufficient to restore a normal, well-defined, typical hepatocyte morphology (Fig. 4j). Furthermore, in the Periodic Acid-Schiff (PAS) staining used for glycogen deposition analysis, the glycogen levels in liver tissues of DB+SA8 group displayed a significant elevation compared with DB+V group (Fig. 4j), indicating that SA8 prevented reduced glycogen synthesis in *db/db* mice. Furthermore, ML-SA8 (4 mg/kg) was able to reduce serum alanine aminotransferase (ALT) (Fig. 4k) and aspartate aminotransferase (AST) levels (Fig. 4l). Notably, ML-SA8 treatment had no effects on body weight (Suppl. Fig.8f), total cholesterol (TC) (Suppl. Fig.8g), serum triglyceride (TG) (Suppl.Fig.8h) and serum creatinine (Suppl.Fig.8i). Collectively, these findings indicate that ML-SA8 alleviates the hallmarks of diabetic phenotypes in *db/db* mice.

Discussion

Lysosomes, a cellular hub in metabolism, protein degradation, and nutrient sensing, play an indispensable role in numerous metabolic pathways and maintaining cellular homeostasis [60]. Emerging evidence implicates lysosomal calcium signaling as a pivotal yet understudied modulator of metabolic homeostasis. In the current study, we found that genetic or

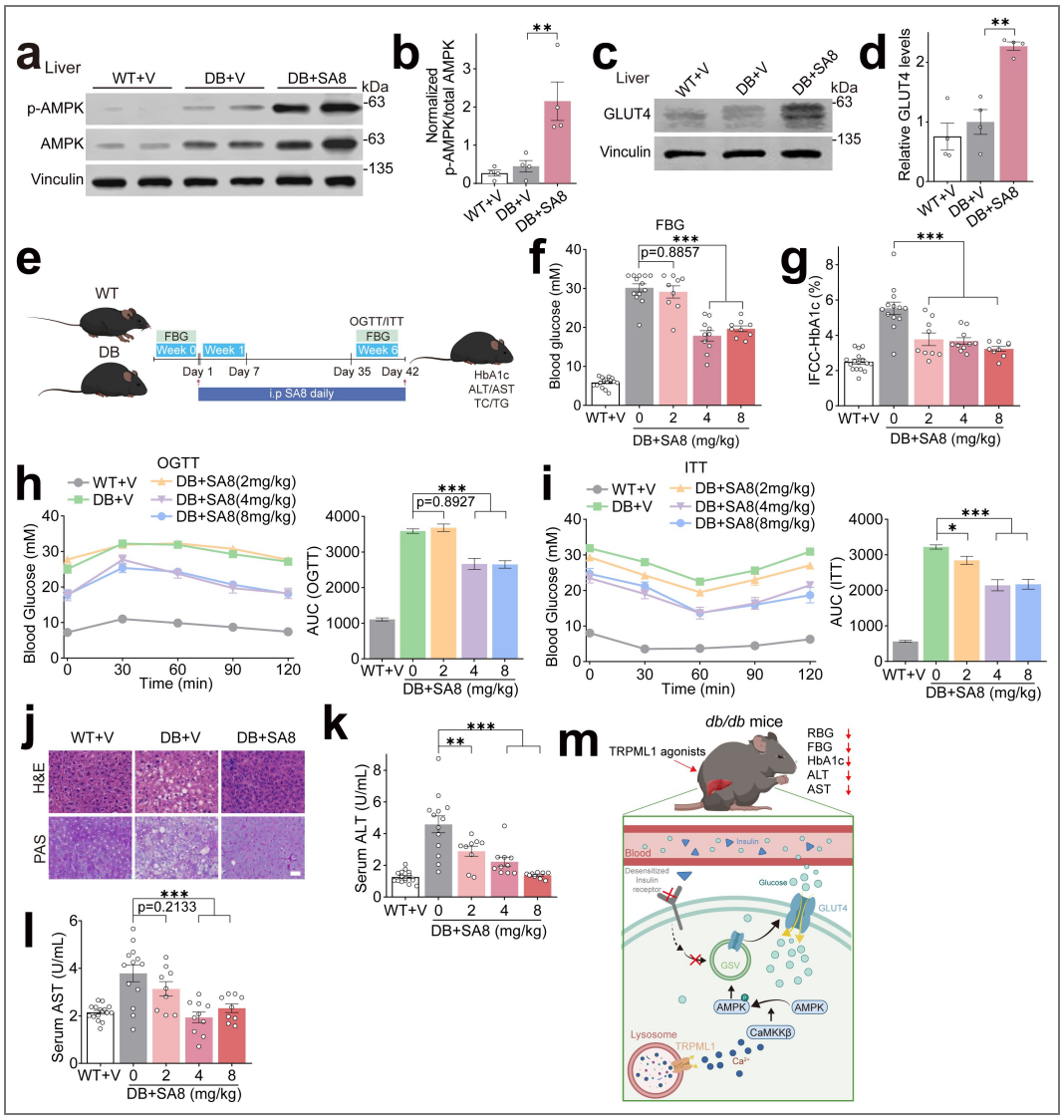

Figure 4. Administration of ML-SA8 attenuates metabolic disorder in *db/db* mice.

(a) ML-SA8 promoted AMPK phosphorylation in the liver tissues of *db/db* mice with ML-SA8 (4 mg/kg) or vehicle (5% DMSO, 90% PEG300, 5% ddH_2O) for 24 h. Liver tissues were collected and extracted proteins were subjected to detect p-AMPK/total AMPK by Western blotting. **(b)** Quantification of results shown in **a**. (n= 4). **(c)** ML-SA8 promoted GLUT4 expression in the liver tissues of *db/db* mice with ML-SA8 (4 mg/kg) or vehicle (5% DMSO, 90% PEG300, 5% ddH_2O) for 6 weeks. Liver tissues were collected and extracted proteins were subjected to detect GLUT4 proteins by Western blotting. **(d)** Quantification of results shown in **c**. (n= 4). **(e)** Experimental design. *db/db* mice were randomly allocated into 4 groups: DB+V group was i.p. injected with vehicle (5% DMSO, 90% PEG300, 5% ddH_2O) daily (n=11); DB+SA8 group was i.p. injected with SA8 (2mg/kg, n=9; 4mg/kg, n=10; 8 mg/kg, n=9). **(f)** Fasting blood glucose (FBG) levels at 0 and 6 weeks. **(g)** HbA1c levels. **(h)** OGTT. Mice daily i.p with SA8 (2, 4, 8 mg/kg) received oral glucose (1g/kg) after 10 h fasting, followed by blood glucose dynamic measurement (0-120 min) with corresponding AUC at the *Right* panel. **(i)** ITT. Mice with SA8 (2, 4, 8 mg/kg) treatment were i.p injected insulin (0.75 U/kg) after 4 h fasting, followed by blood glucose measurements. Left panel: Blood glucose levels (0-120 min). Right panel: AUC values. **(j)** Representative photomicrographs of H&E and PAS staining in liver tissues from mice treated with SA8 (4 mg/kg). Scale bar, 40 μm. **(k)** Serum ALT levels. **(l)** Serum AST levels. All data are presented as mean ± s.e.m.; *$p < 0.05$, **$p < 0.01$, ***$p < 0.001$, ANOVA. **(m)** Pharmacological up-regulation of TRPML1 ameliorates diabetic phenotypes *in vivo* through Ca^{2+}-dependent AMPK activation. ML-SA8 (a specific TRPML1 agonist) activates lysosomal TRPML1 channel, leading to lysosomal Ca^{2+} release from lysosomes. Ca^{2+} triggers Ca^{2+}- dependent AMPK phosphorylation and initiates GLUT4 Storage Vesicle (GSV) trafficking to the PM. Subsequently, extracellular glucose is transferred into cells via GLUT4 and blood glucose levels are reduced *in vitro* and *in vivo*.

pharmacological activation of the lysosomal Ca^{2+} channel-TRPML1 exhibited glucose-lowering effects in both *in vitro* and *in vivo* diabetic models. TRPML1 activation led to AMPK phosphorylation via a Ca^{2+}-CaMKKβ-dependent mechanism and promoted GLUT4 translocation, thereby facilitating glucose influx to reduce hyperglycemia and other phenotypes of T2DM (Fig. 4m). Hence, our proof-of-concept study highlighted TRPML1 as a functional therapeutic target for T2DM and provided evidence that small-molecule TRPML1 agonists may have broad therapeutic potential.

Lysosomal Ca^{2+} is a key regulator for various lysosomal functions i.e., lysosomal exocytosis, membrane trafficking, catabolite export, ion homeostasis and nutrient sensing [61]. Ca^{2+} in the lysosomal lumen is about ~ 0.5 mM, approximately 5,000-fold higher than cytosolic Ca^{2+} (~100 nM). TRPML1 is predominantly localizes on the membranes of late endosomes and lysosomes (LELs) in all mammalian cell types [62]. The related TRPML2 and TRPML3 channels are also permeable to Ca^{2+}, but are more restrictively expressed [62]. TRPML channels play essential roles in various lysosomal functions and respond to a variety of stimuli, such as pH, nutrients and cellular stress, as well as to small molecules [46], suggesting that TRPML1 activities can be specifically modulated. The synthetic agonists (ML-SAs) and inhibitors (ML-SIs) that specifically targeting TRPML1 directly bind to TRPML1 protein in the atomic-resolution co-structures [30, 31]. Notably, the concentration of ML-SAs used in this study has no cytotoxicity towards the cell lines we used including HepG2, HeLa and HAP1 cells (Suppl. Fig.9a, b).

Although GLUT4 is abundant in skeletal muscle, fat, and heart but low in the liver (where GLUT2 predominates) [38], it regulates hepatic glucose homeostasis [63]. Under basal conditions, GLUT4 resides intracellularly and translocates to the PM upon insulin or other stimuli to drive glucose uptake[63]. Given that GLUT4 mediates AMPK-dependent glucose uptake via translocation [37], we examined the effect of ML-SA8 on GLUT4 localization and expression. While our findings support ML-SA-mediated regulation of GLUT4, a GLUT2 - dominant contribution cannot be excluded.

The MiT/TFE family includes TFEB, TFE3, MITF and TFEC. TFEB, TFE3 and MITF, but not TFEC are master regulators of lysosome and autophagy by controlling the “coordinated lysosomal expression and regulation” (CLEAR) network, covering genes associated to lysosomal exocytosis and biogenesis, and autophagy [55, 64, 65]. TFEB/TFE3/MITF are phosphorylated by MTOR (mechanistic target of rapamycin kinase) and then bind to YWHA/14-3-3 in the cytosol inactively [66, 67]. Whereas, under stress conditions i.e. starvation, TFEB/TFE3/MITF are dephosphorylated and actively translocate into nucleus, promoting the expression of genes [56, 68, 69]. TRPML1-released Ca^{2+} release reportedly activates calcineurin, which binds and dephosphorylates TFEB, thus promoting its nuclear translocation [69]. Interestingly, we found that AMPK is not required for TFEB nuclear translocation induced by ML-SA8 (Suppl. Fig.7d, e). Furthermore, by using TFEB/TFE3/MITF TKO cells we found that knockout TFEB/TFE3/MITF has no effect on ML-SA8-induced AMPK activation (Suppl. Fig.7a-c). These results suggest that TRPML1-mediated activation of TFEB and AMPK may be through distinct independent pathways.

In summary, we show a novel AMPK activation pathway via the lysosomal TRPML1-Ca^{2+}-CaMKKβ axis. Pharmacological activation of TRPML1 can efficiently diminish diabetic phenotypes in both *in vitro* and *in vivo* models by targeting AMPK. Hence, targeting lysosomal Ca^{2+} channels i.e. TRPML1 may represent a promising approach to treat T2DM and related metabolic diseases.

Methods and materials

Cell lines and cell culture

HeLa (*RRID: CVCL-0030*), HepG2 (*RRID:CVCL_A8FT*) and C2C12 (*RRID: CVCL-0188*) cells were purchased from American Type Culture Collection (ATCC). Huh7 (*RRID: CVCL-0336*) cells were purchased from Thermo Scientific. HepG2, Huh7 and C2C12 cells were cultured in Dulbecco’s modified Eagle’s medium (DMEM; Thermo Scientific, 11195-065) supplemented with 10% fetal bovine serum (Thermo Scientific, 10091148) and 1% Penicillin-Streptomycin (PS; Solarbio, P1400). HeLa cells were maintained in modified Eagle’s medium (MEM; Thermo Scientific, 1964643) supplemented with 10% FBS and 1% PS. GFP-TFEB HeLa stable, HAP1 (*RRID: CVCL-Y019*,

Horizon Company), *TRPML1* KO HAP1, HEK293-GCaMP7-TRPML1 and *ATG5* KO HAP1 cells were maintained in our laboratory as previously described [45, 56, 70, 71] and cultured in Iscove's Modified Dulbecco's Medium (IMDM; Gibco, 6123179) supplemented with 10% FBS and 1% PS. All cells were used after in-house authentication for mycoplasma contamination and maintained at 37 °C in a humidified 5% CO_2 incubator. Cells with passage number less than 20 were used in this study.

Construction of insulin resistance (IR) model

PA (Sigma-Aldrich, P0500) was applied to construct the IR model [72]. Briefly, 9.2 mg PA was completely dissolved in 1ml of 0.1 M NaOH by warming to 80 ℃ until becoming transparent and clear. The PA solution was further diluted in fatty acid-free bovine serum albumin solution (BSA, 0.325 g BSA dissolved in 8 ml of 0.9 % NaCl by heating at 45℃). The two solutions were then mixed with gentle agitation to get final PA stock solution (4 mM), which was further sterilized by passing through 0.22 μm filters, aliquoted and stored at -20 ℃. Cells were cultured at approximately 70% confluency and treated with PA (0.25 mM, 12 h) to construct IR model, followed by chemical treatment as required conditions.

Plasmid transfection

Plasmids TRPML1-mCherry and GFP-TRPML1 were maintained in our laboratory [73]. Cells were seeded into 6-well plates and transfected with plasmids using Lipofectamine 3000 (Thermo Scientific, 2163785). The efficiency of the transfection was validated by Western blotting or Q-PCR.

RNA interference

The siRNA sequences targeting human CaMKKβ (5′-GGA CCA UCU GUA CAU GGU GUU CGA A-3′) were chemically synthesized by GenePharma. HepG2 cells were seeded into 6-well plates and transfected with siRNA using Lipofectamine RNAi-Max reagent (Thermo Fisher Scientific, 13778150). The efficiency of the siRNA knockdown was assayed by Q-PCR.

RNA extraction and Q-PCR

Total RNA was isolated from cells using Trizol (Thermo Scientific, 191002), and cDNA was generated using the GoScript Reverse Transcription System (Promega, 0000316057) according to the manufacturer's protocol. Q-PCR was performed using the SYBR Green Mix (TOYOBO, 563700) in CFX Connect Optics (Bio-Rad). The changes in the mRNA expression of target genes were normalized to that of the housekeeping gene HPRT. Primer sequences used in this study are listed below:

HPRT; For 5′-TGGCGTCGTGATTAGTGATG-3′, Rev 5′-CTGTTCTCGTCCAGCA GACACT-3′

CaMKKβ; For 5′- TCCAGACCACGACATAG -3′, Rev 5′-CAGGGGTGCAGCTTGATTTC-3′

GCaMP7 Ca^{2+} imaging

GCaMP7 Ca^{2+} imaging was performed in HEK293 cells stably expressing GCaMP7-TRPML1, a lysosome-targeted genetically-encoded Ca^{2+} sensor [70]. Cells were excited at 488 nm, and the emission fluorescence was recorded at 510 nm using a FlexStation 3 scanning fluorometer. Fluorescence intensity at 488 nm excitation (F_{488}) was acquired at regular intervals under controlled temperature (e.g., 37 °C) and continuous perfusion with appropriate buffer. Data were normalized to baseline fluorescence (F_0) and presented as $\Delta F/F_0$.

Immunofluorescence and confocal imaging

For immunofluorescence detection of GLUT4, cells were grown and stained on coverslips in 24-well plates. 4% paraformaldehyde (Solarbio, P1110) was added to each well and cells were fixed for 15 min at room temperature. 0.3% Triton X-100 (Sigma-Aldrich, T8787) was used for permeabilization for 10 min, followed by 1 h blocking with 1% bovine serum albumin (Sigma-Aldrich, WXBC2612V) in phosphate-buffered saline (PBS; Thermo Scientific, 21600069). The cells

were incubated overnight at 4°C with anti-GLUT4 antibodies (Abcam, AB33780) (1:1000). After washing for 5 times with PBS, secondary antibodies conjugated to Alexa Fluor -488 (Thermo Scientific, 1705869) (1:1000) were added and incubated for 2 h in a dark place. DAPI (Sigma-Aldrich, D9542) was added to stain nuclei for 15 min and briefly washed for 3 times. Coverslips were then mounted with Fluoromount-G (Southern Biotech) and images were acquired with an Olympus or Zeiss confocal microscope.

Measurement of cellular glucose uptake

Cellular glucose uptake was measured using a fluorescence-labeled glucose analogue-2-NBDG (MCE, 186689-07-6) [44]. Briefly, cells were seeded about 70% confluency and treated with chemicals as required conditions. Cells were then washed and fresh DMEM (no glucose, no FBS, no phenol red, Solarbio, D6540) containing 50 μM 2-NBDG was added for 30 min, followed by PBS wash three times. The fluorescence was visualized with an Olympus IX-73 inverted microscope. Fluorescence intensity was quantified using Image J software.

Measurement of extracellular glucose consumption

Glucose consumption in the medium was measured using a glucose consumption kit (Nanjing Jiancheng Bioengineering Institute, A154-1-1) [74]. Cells were seeded in a 6-well plate at a density of 1×10^6 cells/ml and treated with chemicals as required conditions in DMEM (no FBS, no phenol red) with 10 mM glucose. After treatment, an aliquot of supernatant medium was added to a 96-well plate. The absorbance was measured at 505 nm with a spectrophotometer VARIOSKAN LUX (Thermo Scientific). Glucose concentration was calculated as: [Medium Glucose] = $[(\text{Sample}_{\text{absorbance}}\text{-blank}_{\text{absorbance}}) / (\text{Standard}_{\text{absorbance}}\text{-blank}_{\text{absorbance}})] \times 5.55$ mmol/L × X, where 5.55 mmol/L is the concentration of the glucose standard, and X is the dilution factor.

Protein extraction and Western blotting

Cells or tissues were lysed in RIPA buffer (Solarbio, R0010) supplemented with 1x protease inhibitors cocktail (Sigma-Aldrich, P8340) (1: 100) and 1 x phosphatase inhibitor cocktail (Abcam, GR304037-28) (1: 100) on ice for 20 min. The membrane protein fraction was extracted using a membrane and cytoplasm protein extraction kit according to manufacturer's protocol (Beyotime, P0033, Shanghai, China). Protein samples were separated by sodium dodecyl sulfate-polyacrylamide gel electrophoresis gels, followed by transferring to polyvinylidene difluoride membranes (Merck, R7DA8778E). The membranes were blocked with 5% nonfat dry milk for 1 h and incubated with antibodies against AMPK (Cell Signaling Technology, 2532) (1:1000), p-AMPK (Cell Signaling Technology, 2535) (1:1000), GLUT4 (Abcam, AB33780) (1:1000), Vinculin (Abcam, AB8226) (1:2000), TFEB (Cell Signaling Technology, 4240S) (1:1000), TFE3 (HPA02300881) (1:1000), MITF (Abcam, AB20663) (1:1000) and GAPDH (Sigma-Aldrich, G9545) (1:10,000), respectively. Bound antibodies were detected horseradish peroxidase-conjugated anti-rabbit (Abcam, ab6721) or anti-mouse secondary antibodies (Abcam, ab6789) (1:10,000) in 5 % nonfat dry milk for 2 h at room temperature with agitation. Protein bands were visualized using enhanced chemiluminescence reagents (Thermo Scientific, 203-17071) in a Li-COR Biosciences Odyssey Fc system. Band intensities were quantified using the Image J software.

Animals

Specific pathogen free (SPF) grade male C57BLKS/J mice (8-week-old) and male C57BLKS/J-Lepr KO (db/db) mice were purchased from GemPharmatech Limited Company (Nanjing, China). Throughout the manuscript, "DB" denotes genetically diabetic db/db mice. Animals were handled according to approved institutional animal care and use committee (IACUC) protocols (20241226208) of Zhejiang University of Technology. Mice were acclimated for one week prior to the experiment. After the acclimation period, mice were randomly assigned to experimental groups. At the end of the experiments, all mice were euthanized by CO_2 inhalation followed by cervical dislocation to confirm death. Blood and liver tissues were rapidly collected for subsequent biochemical and molecular analyses. All experimental procedures were conducted in accordance

with the Guide for the Care and Use of Laboratory Animals in the Zhejiang University of Technology, Hangzhou, China, and conformed to the National Institutes of Health Guide for Care and Use of Laboratory Animals.

Histopathological analysis (H&E and PAS staining)

Liver sections were fixed in 4 % paraformaldehyde buffer and embedded in paraffin. Liver slices were then deparaffinized, rehydrated, and stained with H&E (Solarbio, G1120) or PAS (Solarbio, G1281). All staining procedures were performed according to standard protocols followed by microscopy examination. The section images were obtained using the Olympus/Zeiss Fluorescence inverted microscope.

Blood glucose and insulin measurements

Oral Glucose Tolerance Test (OGTT) and Insulin Tolerance Test (ITT) were performed on each group of mice. For OGTT, mice fasted for 10 h received oral glucose (1g/kg). For ITT, mice fasted for 4 h received i.p. injection of insulin (0.75 U /kg). Tail blood glucose was measured at 0, 30, 60, 90, and 120 min post-administration. Random blood glucose (RBG) was measured every four days (9:00–11:00 AM) to assess non-fasted status, minimizing circadian variation. Fasting blood glucose (FBG) was measured at baseline (Week 0) and endpoint (Week 6) after 6 h fast. Blood glucose was determined using a Sinocare glucometer, and plasma insulin by an ultrasensitive insulin ELISA kit (Solarbio, SEKM-0141). Area under the curve (AUC) was calculated for glucose response. Blood samples were collected through mice tail. After sterilizing the tail with an alcohol swab, a small incision was made at the tail vein tip after discarding the first droplet.

Reagents

Chemicals used in this study including BAPTA-AM (Thermo Scientific, 1824047), EGTA-AM (Sigma-Aldrich, E3478), DFO (MCE, HY-B0988), TPEN (MCE, HY-100202), GPN (Santa Cruz Biotech, sc-252858), riluzole (Sigma-Aldrich, R116), PA (Sigma-Aldrich, P0500), insulin (Beyotime, P3376), metformin (Beyotime, S1741), CC (MCE, HY-13418A), STO609 (MCE, HY-19805), TG assay (Solarbio, BC0625), TC assay (Solarbio, BC1985), ALT assay (Solarbio, BC1555), AST assay (Solarbio, BC1565), HbA1c kit (Solarbio, BC5615), Creatinine assay (Nanjing Jiancheng Company, C011-2-1). ML-SA5, ML-SA8 and ML-SI5 were custom synthesized (available upon MTA request).

Statistical analysis

Data are presented as mean ± s.e.m. from at least 3 independent experiments. Statistical comparisons were performed using a two tailed *Student's t-test* (paired or unpaired as appropriate) or one-way/two-way ANOVA followed by Tukey's or Dunnett's post hoc test for multiple comparisons. A P value < 0.05 was considered statistically significant.

Data availability

All data generated or analyzed during this study are included in the manuscript and supporting files

Acknowledgements

This work was supported by a grant from National Natural Science Foundation of China (31600823 to D. L.). Additional support was provided by Calygene Biotechnology Inc. (XT [2016]008@) and Lysoway Therapeutics, Inc. (KYY-HX-20210129). The funders had no role in study design, data collection and analysis, decision to publish, or preparation of the manuscript. We appreciate the encouragement and assistance provided by Dr. Haoxing Xu and his laboratory members. The authors thanks Experimental Animal Center of Zhejiang University of Technology for providing the animal facilities and technical support for this study.

Additional information

Author contributions

J.Z., Data curation, Investigation, Methodology and Writing original draft; Z.P., Data curation, Validation, Investigation, Methodology and Writing original draft, review and editing; S.W., Data curation, Investigation, Methodology and Writing review and editing; H.Z., Data curation, Methodology, Writing review and editing; Y.W., Z.D., Q.W., Investigation, Methodology; D.L., Conceptualization, Supervision, Funding acquisition, Validation, Investigation, Methodology, Project administration, Writing original draft, review and finalization.

Abbreviations

ALT: alanine aminotransferase
AMP: adenosine monophosphate
AMPK: AMP-activated protein kinase
ANOVA: analyses of variance
AST: aspartate aminotransferase
BAPTA-AM: 1,2-bis(2-aminophenoxy)ethane-N,N,N′,N′-tetraacetic acid tetrakis-acetoxymethyl ester
CaMKKβ: calcium/calmodulin-dependent protein kinase kinase β
DFO: deferoxamine mesylate
EGTA-AM: EGTA Acetoxymethyl ester
ER: endoplasmic reticulum
FBG: fasting blood glucose
FBS: fetal bovine serum
GLUT4: Glucose Transporter 4
GPN: Glycyl-L-phenylalanine 2-naphthylamide
HbA1c: hemoglobin A1c
H&E: hematoxylin-eosin
ITT: insulin tolerance test
IR: insulin resistance
KO: knockout
LKB1: liver kinase B1
MCOLN1/TRPML1: mucolipin 1
MET: metformin
ML-SA8: mucolipin-specific synthetic agonist 8
ML-SI5: mucolipin-specific synthetic inhibitor 5
OGTT: oral glucose tolerance test
PA: palmitic acid
PAS: periodic acid-schiff
PBS: phosphate-buffered saline
Q-PCR: quantitative real time polymerase chain reaction
RBG: random blood glucose
TFEB: transcription factor EB
TG: triglyceride
TC: total cholesterol
TPCs: two-pore channels
TPEN: N,N,N′,N′-tetrakis (2-pyridylmethyl) ethylene-diamine
T2DM: type 2 diabetes mellitus
ULK1: Unc like autophagy activating kinase 1
WT: wild-type
2-NBDG: 2-deoxy-2-[(7-nitro-2,1,3-benzoxadiazol-4-yl)amino]-d-glucose

Funding

Funder	Grant reference number	Author
MOST | National Natural Science Foundation of China (NSFC)	31600823	Dan Li

Author ORCID iDs

Dan Li: https://orcid.org/0000-0002-7316-5151

Additional files

Supplementary figures

References

1. **Ahmad E,** et al. (2022) Type 2 diabetes. *Lancet* **400**:1803-1820 https://doi.org/10.1016/s0140-6736(22)01655-5 | PubMed
2. **Sun H,** et al. (2022) IDF Diabetes Atlas: Global, regional and country-level diabetes prevalence estimates for 2021 and projections for 2045. *Diabetes Res Clin Pract* **183**:109119 https://doi.org/10.1016/j.diabres.2021.109119 | PubMed
3. **González A,** et al. (2020) AMPK and TOR: The Yin and Yang of Cellular Nutrient Sensing and Growth Control. *Cell Metab* **31**:472-492 https://doi.org/10.1016/j.cmet.2020.01.015 | PubMed
4. **Hardie DG** (2018) Keeping the home fires burning: AMP-activated protein kinase. *J R Soc Interface* **15** https://doi.org/10.1098/rsif.2017.0774 | PubMed
5. **Woods A,** et al. (2005) Ca2+/calmodulin-dependent protein kinase kinase-beta acts upstream of AMP-activated protein kinase in mammalian cells. *Cell Metab* **2**:21-33 https://doi.org/10.1016/j.cmet.2005.06.005 | PubMed
6. **Ross FA,** Jensen TE, Hardie DG (2016) Differential regulation by AMP and ADP of AMPK complexes containing different gamma subunit isoforms. *Biochem J* **473**:189-99 https://doi.org/10.1042/bj20150910 | PubMed
7. **Hawley SA,** et al. (2003) Complexes between the LKB1 tumor suppressor, STRAD alpha/beta and MO25 alpha/beta are upstream kinases in the AMP-activated protein kinase cascade. *J Biol* **2**:28 https://doi.org/10.1186/1475-4924-2-28 | PubMed
8. **Clapham DE** (2007) Calcium signaling. *Cell* **131**:1047-58 https://doi.org/10.1016/j.cell.2007.11.028 | PubMed
9. **Scotto Rosato A,** et al. (2019) TRPML1 links lysosomal calcium to autophagosome biogenesis through the activation of the CaMKKβ/VPS34 pathway. *Nat Commun* **10**:5630 https://doi.org/10.1038/s41467-019-13572-w | PubMed
10. **Zhong XZ,** et al. (2016) BK channel agonist represents a potential therapeutic approach for lysosomal storage diseases. *Sci Rep* **6**:33684 https://doi.org/10.1038/srep33684 | PubMed
11. **Somogyi A,** et al. (2023) The synthetic TRPML1 agonist ML-SA1 rescues Alzheimer-related alterations of the endosomal-autophagic-lysosomal system. *J Cell Sci* **136** https://doi.org/10.1242/jcs.259875 | PubMed
12. **Bae M,** et al. (2014) Activation of TRPML1 clears intraneuronal Abeta in preclinical models of HIV infection. *J Neurosci* **34**:11485-503 https://doi.org/10.1523/jneurosci.0210-14.2014 | PubMed
13. **Bargal R,** et al. (2000) Identification of the gene causing mucolipidosis type IV. *Nat Genet* **26**:118-23 https://doi.org/10.1038/79095 | PubMed
14. **Pu J** (2022) Targeting the lysosome: Mechanisms and treatments for nonalcoholic fatty liver disease. *J Cell Biochem* **123**:1624-1633 https://doi.org/10.1002/jcb.30274 | PubMed

15. **Arden C,** et al. (2024) Autophagy and lysosomal dysfunction in diabetes and its complications. *Trends Endocrinol Metab* **35**:1078-1090 https://doi.org/10.1016/j.tem.2024.06.010 | PubMed

16. **Spampanato C,** et al. (2013) Transcription factor EB (TFEB) is a new therapeutic target for Pompe disease. *EMBO Mol Med* **5**:691-706 https://doi.org/10.1002/emmm.201202176 | PubMed

17. **Feng X,** et al. (2025) Activation of lysosomal Ca2+ channels mitigates mitochondrial damage and oxidative stress. *J Cell Biol* **224** https://doi.org/10.1083/jcb.202403104 | PubMed

18. **Yu L,** et al. (2020) Small-molecule activation of lysosomal TRP channels ameliorates Duchenne muscular dystrophy in mouse models. *Sci Adv* **6**:eaaz2736 https://doi.org/10.1126/sciadv.aaz2736 | PubMed

19. **Chen CC,** et al. (2014) A small molecule restores function to TRPML1 mutant isoforms responsible for mucolipidosis type IV. *Nat Commun* **5**:4681 https://doi.org/10.1038/ncomms5681 | PubMed

20. **Shi W,** et al. (2018) Saikosaponin-d inhibits proliferation by up-regulating autophagy via the CaMKKβ–AMPK–mTOR pathway in ADPKD cells. *Molecular and Cellular Biochemistry* **449**:219-226 https://doi.org/10.1007/s11010-018-3358-0 | PubMed

21. **Vahidi Ferdowsi P,** et al. (2021) TRPV1 Activation by Capsaicin Mediates Glucose Oxidation and ATP Production Independent of Insulin Signalling in Mouse Skeletal Muscle Cells. *Cells* **10**:1560 https://doi.org/10.3390/cells10061560 | PubMed

22. **Morgan AJ,** et al. (2011) Molecular mechanisms of endolysosomal Ca2+ signalling in health and disease. *Biochem J* **439**:349-74 https://doi.org/10.1042/bj20110949 | PubMed

23. **Prins D,** Michalak M (2011) Organellar calcium buffers. *Cold Spring Harb Perspect Biol* **3**:a004069 https://doi.org/10.1101/cshperspect.a004069 | PubMed

24. **Hawley SA,** et al. (1996) Characterization of the AMP-activated protein kinase kinase from rat liver and identification of threonine 172 as the major site at which it phosphorylates AMP-activated protein kinase. *J Biol Chem* **271**:27879-87 https://doi.org/10.1074/jbc.271.44.27879 | PubMed

25. **Hu M,** et al. (2024) The ion channels of endomembranes. *Physiol Rev* **104**:1335-1385 https://doi.org/10.1152/physrev.00025.2023 | PubMed

26. **Wang X,** et al. (2012) TPC proteins are phosphoinositide- activated sodium-selective ion channels in endosomes and lysosomes. *Cell* **151**:372-83 https://doi.org/10.1016/j.cell.2012.08.036 | PubMed

27. **Du W,** et al. (2021) Lysosomal Zn(2+) release triggers rapid, mitochondria-mediated, non-apoptotic cell death in metastatic melanoma. *Cell Rep* **37**:109848 https://doi.org/10.1016/j.celrep.2021.109848 | PubMed

28. **Zhou G,** et al. (2001) Role of AMP-activated protein kinase in mechanism of metformin action. *J Clin Invest* **108**:1167-74 https://doi.org/10.1172/jci13505 | PubMed

29. **Sahoo N,** et al. (2017) Gastric Acid Secretion from Parietal Cells Is Mediated by a Ca2+ Efflux Channel in the Tubulovesicle. *Developmental Cell* **41**:262-273. https://doi.org/10.1016/j.devcel.2017.04.003 | PubMed

30. **Schmiege P,** et al. (2017) Human TRPML1 channel structures in open and closed conformations. *Nature* **550**:366-370 https://doi.org/10.1038/nature24036 | PubMed

31. **Schmiege P,** Fine M, Li X (2021) Atomic insights into ML-SI3 mediated human TRPML1 inhibition. *Structure* **29**:1295-1302. https://doi.org/10.1016/j.str.2021.06.003 | PubMed

32. **Zhang X,** et al. (2019) Agonist-specific voltage-dependent gating of lysosomal two-pore Na(+) channels. *eLife* **8** https://doi.org/10.7554/elife.51423 | PubMed

33. **Beltran-Parrazal L,** Charles A (2003) Riluzole inhibits spontaneous Ca2+ signaling in neuroendocrine cells by activation of K+ channels and inhibition of Na+ channels. *Br J Pharmacol* **140**:881-8 https://doi.org/10.1038/sj.bjp.0705491 | PubMed

34. **Albertini C,** et al. (2022) Riluzole–Rasagiline Hybrids: Toward the Development of Multi-Target-Directed Ligands for Amyotrophic Lateral Sclerosis. *ACS Chemical Neuroscience* **13**:2252-2260 https://doi.org/10.1021/acschemneuro.2c00261 | PubMed

35. **Dolfi SC,** et al. (2017) Riluzole exerts distinct antitumor effects from a metabotropic glutamate receptor 1-specific inhibitor on breast cancer cells. *Oncotarget* **8**:44639-44653 https://doi.org/10.18632/oncotarget.17961 | PubMed

36. **Kakoti BB,** et al. (2024) AMPK pathway: an emerging target to control diabetes mellitus and its related complications. *J Diabetes Metab Disord* **23**:441-459 https://doi.org/10.1007/s40200-024-01420-8 | PubMed

37. **Addinsall AB,** et al. (2022) Electrical stimulated GLUT4 signalling attenuates critical illness-associated muscle wasting. *J Cachexia Sarcopenia Muscle* **13**:2162-2174 https://doi.org/10.1002/jcsm.12978 | PubMed

38. **Karim S,** Adams DH, Lalor PF (2012) Hepatic expression and cellular distribution of the glucose transporter family. *World J Gastroenterol* **18**:6771-81 https://doi.org/10.3748/wjg.v18.i46.6771 | PubMed

39. **He C,** et al. (2023) Natural exosomes-like nanoparticles in mung bean sprouts possesses anti-diabetic effects via activation of PI3K/Akt/GLUT4/GSK-3β signaling pathway. *J Nanobiotechnology* **21**:349 https://doi.org/10.1186/s12951-023-02120-w | PubMed

40. **Kurabayashi A,** et al. (2022) Murine remote ischemic preconditioning upregulates preferentially hepatic glucose transporter-4 via its plasma membrane translocation, leading to accumulating glycogen in the liver. *Life Sci* **290**:120261 https://doi.org/10.1016/j.lfs.2021.120261 | PubMed

41. **Hu W,** et al. (2022) Hirsutine ameliorates hepatic and cardiac insulin resistance in high-fat diet-induced diabetic mice and in vitro models. *Pharmacol Res* **177**:105917 https://doi.org/10.1016/j.phrs.2021.105917 | PubMed

42. **Samuel VT,** Shulman GI (2012) Mechanisms for insulin resistance: common threads and missing links. *Cell* **148**:852-71 https://doi.org/10.1016/j.cell.2012.02.017 | PubMed

43. **Xiao H,** et al. (2022) Gentiopicroside targets PAQR3 to activate the PI3K/AKT signaling pathway and ameliorate disordered glucose and lipid metabolism. *Acta Pharm Sin B* **12**:2887-2904 https://doi.org/10.1016/j.apsb.2021.12.023 | PubMed

44. **Yamada K,** et al. (2000) Measurement of glucose uptake and intracellular calcium concentration in single, living pancreatic beta-cells. *J Biol Chem* **275**:22278-83 https://doi.org/10.1074/jbc.m908048199 | PubMed

45. **Qi J,** et al. (2021) MCOLN1/TRPML1 finely controls oncogenic autophagy in cancer by mediating zinc influx. *Autophagy* **17**:4401-4422 https://doi.org/10.1080/15548627.2021.1917132 | PubMed

46. **Dong X.-P,** et al. (2008) The type IV mucolipidosis-associated protein TRPML1 is an endolysosomal iron release channel. *Nature* **455**:992-996 https://doi.org/10.1038/nature07311 | PubMed

47. **Marcelo KL,** Means AR, York B (2016) The Ca 2+ /Calmodulin/CaMKK2 Axis: Nature's Metabolic CaMshaft. *Trends in Endocrinology & Metabolism* **27**:706-718 https://doi.org/10.1016/j.tem.2016.06.001 | PubMed

48. **Medina DL,** et al. (2015) Lysosomal calcium signalling regulates autophagy through calcineurin and TFEB. *Nat Cell Biol* **17**:288-99 https://doi.org/10.1038/ncb3114 | PubMed

49. **Hay JC** (2007) Calcium: a fundamental regulator of intracellular membrane fusion?. *EMBO reports* **8**:236-240 https://doi.org/10.1038/sj.embor.7400921 | PubMed

50. **Radford RJ,** Lippard SJ (2013) Chelators for investigating zinc metalloneurochemistry. *Curr Opin Chem Biol* **17**:129-36 https://doi.org/10.1016/j.cbpa.2013.01.009 | PubMed

51. **Pramanik S,** et al. (2019) Cell Permeable Imidazole-Desferrioxamine Conjugates: Synthesis and In Vitro Evaluation. *Bioconjug Chem* **30**:841-852 https://doi.org/10.1021/acs.bioconjchem.8b00924 | PubMed

52. **Hawley SA,** et al. (2005) Calmodulin-dependent protein kinase kinase-beta is an alternative upstream kinase for AMP-activated protein kinase. *Cell Metab* **2**:9-19 https://doi.org/10.1016/j.cmet.2005.05.009 | PubMed

53. **Kim J,** et al. (2016) AMPK activators: mechanisms of action and physiological activities. *Exp Mol Med* **48**:e224 https://doi.org/10.1038/emm.2016.16 | PubMed

54. **Tokumitsu H,** et al. (2002) STO-609, a specific inhibitor of the Ca(2+)/calmodulin-dependent protein kinase kinase. *J Biol Chem* **277**:15813-8 https://doi.org/10.1074/jbc.m201075200 | PubMed

55. **Napolitano G,** Ballabio A (2016) TFEB at a glance. *J Cell Sci* **129**:2475-81 https://doi.org/10.1242/jcs.146365 | PubMed

56. **Zhang X,** et al. (2016) MCOLN1 is a ROS sensor in lysosomes that regulates autophagy. *Nat Commun* **7**:12109 https://doi.org/10.1038/ncomms12109 | PubMed

57. **Paquette M,** et al. (2021) AMPK-dependent phosphorylation is required for transcriptional activation of TFEB and TFE3. *Autophagy* **17**:3957-3975 https://doi.org/10.1080/15548627.2021.1898748 | PubMed

58. **Sardiello M,** et al. (2009) A gene network regulating lysosomal biogenesis and function. *Science* **325**:473-7 https://doi.org/10.1126/science.1174447 | PubMed

59. **Suriano F,** et al. (2021) Novel insights into the genetically obese (ob/ob) and diabetic (db/db) mice: two sides of the same coin. *Microbiome* **9**:147 https://doi.org/10.1186/s40168-021-01097-8 | PubMed

60. **Lawrence RE,** Zoncu R (2019) The lysosome as a cellular centre for signalling, metabolism and quality control. *Nat Cell Biol* **21**:133-142 https://doi.org/10.1038/s41556-018-0244-7 | PubMed

61. **Xu H,** Ren D (2015) Lysosomal physiology. *Annu Rev Physiol* **77**:57-80 https://doi.org/10.1146/annurev-physiol-021014-071649 | PubMed

62. **Cheng X,** et al. (2010) Mucolipins: Intracellular TRPML1-3 channels. *FEBS Lett* **584**:2013-21 https://doi.org/10.1016/j.febslet.2009.12.056 | PubMed

63. **Huang S,** Czech MP (2007) The GLUT4 glucose transporter. *Cell Metab* **5**:237-52 https://doi.org/10.1016/j.cmet.2007.03.006 | PubMed

64. **Martini-Stoica H,** et al. (2016) The Autophagy-Lysosomal Pathway in Neurodegeneration: A TFEB Perspective. *Trends Neurosci* **39**:221-34 https://doi.org/10.1016/j.tins.2016.02.002 | PubMed

65. **Sardiello M,** Ballabio A (2009) Lysosomal enhancement: a CLEAR answer to cellular degradative needs. *Cell Cycle* **8**:4021-2 https://doi.org/10.4161/cc.8.24.10263 | PubMed

66. **Martina JA,** Rosa P (2018) Protein phosphatase 2A stimulates activation of TFEB and TFE3 transcription factors in response to oxidative stress. *Journal of Biological Chemistry* **293** https://doi.org/10.1074/jbc.ra118.003471 | PubMed

67. **Napolitano G,** et al. (2018) mTOR-dependent phosphorylation controls TFEB nuclear export. *Nat Commun* **9**:3312 https://doi.org/10.1038/s41467-018-05862-6 | PubMed

68. **Puertollano R,** et al. (2018) The complex relationship between TFEB transcription factor phosphorylation and subcellular localization. *EMBO J* **37** https://doi.org/10.15252/embj.201798804 | PubMed

69. **Medina DL,** Di Paola S, Peluso I, Armani A, De Stefani D, Venditti R, Montefusco S, Scotto-Rosato A, Prezioso C, Forrester A, *et al.* (2015) Lysosomal calcium signalling regulates autophagy through calcineurin and TFEB. *Nat Cell Biol* **17**:288-99 https://doi.org/10.1038/ncb3114 | PubMed

70. **Li D,** et al. (2021) Sulforaphane Activates a lysosome-dependent transcriptional program to mitigate oxidative stress. *Autophagy* **17**:872-887 https://doi.org/10.1080/15548627.2020.1739442 | PubMed

71. **Shen D,** et al. (2012) Lipid storage disorders block lysosomal trafficking by inhibiting a TRP channel and lysosomal calcium release. *Nat Commun* **3**:731 https://doi.org/10.1038/ncomms1735 | PubMed

72. **Lee JY,** Cho HK, Kwon YH (2010) Palmitate induces insulin resistance without significant intracellular triglyceride accumulation in HepG2 cells. *Metabolism* **59**:927-34 https://doi.org/10.1016/j.metabol.2009.10.012 | PubMed

73. **Samie M,** et al. (2013) A TRP channel in the lysosome regulates large particle phagocytosis via focal exocytosis. *Dev Cell* **26**:511-24 https://doi.org/10.1016/j.devcel.2013.08.003 | PubMed

74. **Kabasakalian P,** Kalliney S, Westcott A (1974) Enzymatic blood glucose determination by colorimetry of N,N-diethylaniline-4 aminoantipyrine. *Clinical chemistry* **20**:606-607 https://doi.org/10.1093/clinchem/20.5.606 | PubMed

75. **Phillippe M,** et al. (1995) Ionomycin-stimulated phasic myometrial contractions. *Am J Physiol* **269**:E779-85 https://doi.org/10.1152/ajpendo.1995.269.4.e779 | PubMed

76. **Treiman M,** Caspersen C, Christensen SB (1998) A tool coming of age: thapsigargin as an inhibitor of sarco-endoplasmic reticulum Ca(2+)-ATPases. *Trends Pharmacol Sci* **19**:131-5 https://doi.org/10.1016/s0165-6147(98)01184-5 | PubMed

Peer reviews

Reviewer #1 (Public review):

Summary:

This article purports to show that ML-SA8, a synthetic activator of the lysosomal TRPML1 channel, results in AMPK activation and glucose uptake in hepatocytes, and that this action has therapeutic potential for metabolic disease. The final figure shows that glucose levels are improved in db/db mice, although it is not entirely clear whether this is due to an effect on the liver, on other tissues, or on glucose production or uptake. The earlier figures try to make the case that SA8 causes activation and GLUT4 translocation and glucose uptake in liver cells; however, these data are not convincing. GLUT4 is expressed at such low levels in liver that it is likely not physiologically important. The authors use a fluorescent glucose analog to measure glucose uptake, and this molecule has been shown to enter cells largely by fluid phase endocytosis. Overall, this reviewer finds the premise misguided and the data unconvincing.

Strengths and Weaknesses:

The initial figures show phosphorylation of AMPK on Thr172, but no downstream effects are shown. Usually, to convincingly show that AMPK activity is increased, it would be appropriate to immunoblot phospho-ACC or some other substrate. This is minor.

Lines 135-148: GLUT4 is not expressed at levels that are significant for physiology in liver cells, and its function in liver is not particularly relevant. The authors cite references 38-40 to support that it may be expressed at low levels in liver, but no knockout studies have been done to show that this expression is physiologically important.

Figure 1e is not convincing. No controls are included to show the specificity of the antibody for immunofluorescent staining. No intracellular GLUT4 is visible in the unstimulated samples.

In Figure 1f, again, the data are not convincing. The bands seem too sharp for GLUT4, which has 12 membrane-spanning domains as well as an N-linked glycosylation, so that it usually runs as a smear.

Figure 1h. Data are not convincing. 2-NBDG is not a valid approach to measure glucose uptake. 2-NBDG enters cells largely via fluid phase endocytosis, and its accumulation is independent of known GLUT inhibitors such as cytochalasin B (Yazdani et al., MBoC 2022; PMID: 35921166; see also PMID: 42287154). The idea that such a bulky derivative of glucose could enter the transporter channel is not compatible with known structural data.

Supplementary Figure 5 uses 2-NBDG glucose uptake again. This reviewer is not convinced that the data reflect transporter-mediated glucose uptake, as suggested by the authors. As well, although palmitate treatment of cells can cause an insulin-resistant-like phenotype in some cell types, this is not characterized in the present work. Finally, as noted, one would not

expect hepatocytes to exhibit insulin-responsive glucose transport. Glycogen synthesis is the main insulin-regulated step that might be affected.

The data in Figures 2b,c,f,g,k,l are not convincing. Again, 2-NBDG is used.

For the glucose consumption measurements in other panels of Figure 2, the methods section states that cells were cultured in 10 mM glucose. What volume was used? It is difficult to believe that a monolayer of cells would consume very much of the glucose that is present in the culture medium. Data are shown as a percent of controls, and look reasonable, but it would be helpful to include absolute as well as relative units.

In Figure 2, in experiments using the TRPML1 KO cells, no panel is shown to demonstrate knockout. The authors cite a previous paper for the construction of these cells, but the control immunoblot should still be shown here.

In Figure 3, controls are missing in the BAPTA experiment in Figure 3a (only SA8-treated cells were treated with BAPTA and with EGTA). Again, it would be helpful to have p-ACC or some other readout of AMPK activity, and not just AMPK phosphorylation. 2NBDG is again used in this figure.

Line 212-213 the text states "considering our finding that TRPML1-mediated Ca2+ release is essential for AMPK activation." This has not been shown. The work uses chelators and does not necessarily indicate a role for TRPML1. The drug may be specific, as suggested by the authors, but the way this phrase is worded is too strong. As well, AMPK was shown to be phosphorylated, but full activation towards its various substrates has not been shown.

Figure 4cd suggests that GLUT4 expression is increased by 2 or 3-fold in the liver of DB+SA8-treated mice, compared to controls. This may be the case, but its abundance is still likely ~1000-fold less in liver compared to skeletal muscle or adipose tissue. This reviewer is still not convinced that this is physiologically relevant. The images in Supplementary Figure 8 suggest a larger increase, but it remains uncertain whether the staining really represents GLUT4.

Data showing that blood glucose and HbA1c are reduced in SA8-treated mice are reasonable, and GTTs and ITTs are shown. Unfortunately, there are no insulin concentrations, and it remains uncertain whether glucose production is reduced or uptake is increased (or if both effects are present).

In the discussion, the authors again state that GLUT4 is present in the liver and that it regulates hepatic glucose homeostasis, and they cite reference 63. This review article does not argue that GLUT4 acts in the liver to regulate hepatic glucose homeostasis, but that its actions in muscle and fat have secondary effects on the liver.

https://doi.org/10.7554/eLife.112056.1.sa2

Reviewer #2 (Public review):

Summary:

The manuscript contains interesting studies suggesting that pharmacological activation of TRPML1 could be useful to treat T2D by increasing glucose uptake via activation of AMPK. Preclinical studies suggest the inhibitor improved blood glucose in Db/Db mice. Ex vivo studies in cell lines examine both pharmacologic and genetic manipulations, both to activate and to inactivate TRPML1, and the results consistently suggest that TRPML1 activates AMPK and increases glucose uptake.

Strengths:

The manuscript is well written, and the studies are carefully performed.

Weaknesses:

All mechanistic studies were performed in transformed cell lines; conclusions would be stronger if performed in primary cells. The in vivo studies were only performed in male mice. Performing metabolic studies in both sexes is standard practice now. Whether the findings would extend to females was not tested and remains uncertain. Some controls are missing, such as plasma membrane loading controls for fractionation studies. The GLUT4 staining was performed after fixation and permeabilization, yet control cells appear to be devoid of intracellular (and all) staining, a confusing result that doesn't reflect the expected biology.

https://doi.org/10.7554/eLife.112056.1.sa1

Reviewer #3 (Public review):

Summary:

Zhu et al. present a proof-of-concept for targeting the lysosomal calcium channel MCOLN1/TRPML1endolysosomal ion channels to restore type 2 diabetes mellitus (T2DM). Using synthetic TRPML1 agonists (ML-SA8) and genetic manipulation, the authors demonstrate that TRPML1 stimulation triggers localized lysosomal calcium release. This calcium efflux sequentially activates CaMKKβ and phosphorylates AMPK at Thr172 in various cell models, including palmitic acid-induced insulin-resistant HepG2 cells. This signaling pathway promotes GLUT4 translocation to the plasma membrane and increases intracellular glucose uptake. When administered daily to diabetic db/db mice over six weeks, ML-SA8 lowers fasting and random blood glucose, improves oral glucose and insulin tolerance tests, reduces hepatic steatosis, and lowers serum ALT and AST levels.

Strengths:

Based on the TFEB-independent pathway activated by TRPML1 and the experimental approaches described by Medina's group (PMID: 31822666), the authors use a combination of pharmacological and genetic tools to dissect such an intracellular signaling pathway. Additionally, the animal experiments show consistent phenotypic improvements across independent metabolic parameters. The ability of ML-SA8 to restore glycogen deposition and clear hepatic lipid accumulation in db/db mice without causing weight loss or overt toxicity provides a strong rationale for exploring lysosomal targets in metabolic disease.

Weaknesses:

(1) The authors focus almost exclusively on hepatic GLUT4 to explain the observed glucose disposal. However, other glucose transporter isoforms such as GLUT2 dominate basal glucose transport. While the authors show increased AMPK phosphorylation in skeletal muscle and adipose tissue, they do not measure GLUT4 translocation or glucose uptake in these primary disposal organs. As a result, attributing systemic glycemic recovery primarily to hepatic GLUT4 translocation overlooks the major physiological roles of peripheral tissues.

(2) In both HepG2 cells and mouse liver tissues, ML-SA8 treatment increases total GLUT4 protein expression in addition to plasma membrane localization. Because total protein pools expand, the enrichment of GLUT4 in plasma membrane fractions cannot be cleanly attributed to acute vesicular translocation alone. The manuscript does not explain the timescale or mechanism behind this rapid total protein upregulation, leaving a mechanistic gap between acute ion channel gating and protein expression.

(3) While the in vitro specificity of ML-SA8 is well-controlled, the systemic animal experiments lack a specific rescue or knockout control. Small-molecule agonists administered intraperitoneally over six weeks can exert off-target effects. Without demonstrating that co-administering the TRPML1 inhibitor ML-SI5 blunts the therapeutic effect in vivo, or showing that ML-SA8 lacks efficacy in TRPML1-null mice, the definitive link between in vivo glycemic recovery and TRPML1 activation remains incomplete.

https://doi.org/10.7554/eLife.112056.1.sa0